Robust Adaptive Back-Stepping Control Approach Using Quadratic Lyapunov Functions for MMC-Based HVDC Digital Twins

Le Liu(✉), Aleksandra Lekić, and Marjan Popov

Delft University of Technology, Delft 2628 CD, The Netherlands
{L.liu-7,A.Lekic,M.Popov}@tudelft.nl

Abstract. Due to its excellent performance, VSC-based high voltage direct current (HVDC) power systems draw significant attention. They are being heavily used in modern industrial applications, such as onshore and offshore wind farms, and for interconnection between asynchronous networks. However, the traditional proportional-integral (PI) control method is not robust enough to track the reference signal quickly and accurately during significant system disturbances. This paper proposes a robust adaptive back-stepping control (BSC) method that secures vulnerable power-electronic equipment. The adaptive BSC controller regulates the sum of capacitor energy, and the AC grid current through decoupled and closed control-loop design. The major advantage of the proposed control approach is the smooth transient response and accurate tracking ability, which is superior to classical control methods. In addition, the proposed methods have the merits of systematic and recursive design methodology and demand a low processing burden for *Lyapunov* functions and control laws. Moreover, the implementation particularities of the proposed approach are illustrated and verified for a power system digital twin using real-time digital simulator (RTDS).

Keywords: MMC · Energy controller · Nonlinear robust control · Adaptive back-stepping control · *Lyapunov* stability · HVDC grids · RTDS · Digital twins

1 Introduction

The Modular Multilevel Converters (MMC) have high reliability, modular structure, high efficiency, and adequate redundancy. Due to the technical excellence of flexibility and reliability, the MMC-based HVDC power system is attracting significant attention in modern industrial applications. It has been increasingly utilized as the solution for wind farms, STATCOMs, HVDC, and energy storage systems [2].

The most pressing technical challenge of MMC is the simultaneous control of state variables, including the AC/DC voltage, sum capacitor voltages, and circulating currents [3]. MMC, being a switching power converter, features a variety of state variables and complex dynamics, which present nonlinear behaviors [4]. Therefore, to accelerate the feasibility of the MMC-based HVDC system, MMCs are supposed to utilize advanced and robust control methods.

T. Margaria and B. Steffen (Eds.): ISoLA 2022, LNCS 13704, pp. 126–138, 2022.
https://doi.org/10.1007/978-3-031-19762-8_9

These control approaches can be divided into linear and nonlinear controllers. Currently, the HVDC system generally adopts a centralized dispatch approach for power management [5]. The active and reactive power control is usually achieved by implementing the cascaded PI controllers, which can track the set-points without steady-state errors. The structure is simple and easy to employ. However, the linear-based PI controller always encounters complex cascade or parallel structures, and decoupling assumptions between control variables. The transient response is generally attained after 100 ms, which is very slow regarding the fast nature of electrical transients in power systems. Additionally, the selection of proportional and integral gain values is complicated.

Hence, there are many open research topics of advanced nonlinear control strategies, which can control multiple variables, within allowable safe boundaries and constraints. One promising approach for nonlinear control of power electronic converters is the Back-Stepping Control (BSC) method. The BSC has the merits of systematic and recursive design methodology. Some approaches are outlined in [6, 7]. A dual-layer back-stepping control method is reported in [6], where the energy controller delivers the set-point to the lower layer controller. However, the controller is configured as STATCOM, and the feasibility of the method in a point-to-point HVDC system is not proven yet. The authors of [7] designed the BSC method based on the simplified transmission model, and the interaction of wind farms is also considered. However, due to the imprecision of the model, the effectiveness of the control needs to be further verified.

This paper proposes an adaptive back-stepping controller for the MMC-based HVDC system to overcome the challenges mentioned above. The BSC is used to control ac gird *d-q* frame currents. The capacitor energy stored in MMC's sub-modules is used as the upper layer control that generates the corresponding set-point for the *d*-axis grid current. The reactive grid side power is used to deliver the desired value to the *q*-axis current. Additional adaptive terms are introduced for each controlling loop to ensure resiliency to the influence of the angular frequency and minimize the steady-state variation. With proper construction of *Lyapunov* functions and control laws, the system stability is guaranteed. The RTDS device is used as the testing environment, and the simulation results present the robustness and effectiveness of the proposed controller.

The outline of this paper is as follows. Section 2 briefly introduces the state variables of the MMC system. Section 3 presents a detailed design approach of the adaptive BSC. Section 4 introduces the studied digital twin in the RTDS environment. Section 5 presents the results of the transient case studies. Finally, meaningful conclusions are provided in Sect. 6.

2 System Description of MMC

As a basis for the MMC model, the classical MMC configuration is briefly recalled in Fig. 1, and the stationary reference frame using $\Sigma - \Delta$ vector representation is introduced. For the adaptive BSC method design, this section aims at obtaining the MMC state variables through simplified steady-state analysis.

In Fig. 1 with N is denoted the number of H-bridge submodules (SMs) in one arm, the equivalent losses are represented as series inductance L_{arm} and resistance R_{arm} forming the connection between DC-terminals and AC-side output. Two identical arms

are connected to the upper (denoted as U) and lower (denoted as L) DC-terminals, forming one leg of each phase $j \in \{a, b, c\}$. The AC-side interface is assumed as an equivalent resistance and inductance, denoted as R_r and L_r, respectively. Each H-bridge SM consists of four semiconductor switches (S_1, S_2, D_1 and D_2) with the antiparallel connected capacitor. The voltage across the capacitor of each SM is recorded as $v_{Cj}^{U,L}$, where items U and L stand for upper and lower, respectively.

Combined with the switching status, each SM can be controlled in three working modes: inserted, bypassed, and blocked. With proper control of switching conditions of all SMs at each phase, one can obtain the multi-level output voltage. In general, the more inserted SMs, the higher the arm-voltage level.

Sub-modules are considered with their average equivalents, and thus, the modulated currents $i_{Mj}^{U,L}$ and voltages $v_{Mj}^{U,L}$, of the upper and lower arm of a generic phase j, are here given by the following equations,

$$v_{Mj}^{U,L} = m_j^{U,L} \cdot v_{Cj}^{U,L},\ i_j^{U,L} = m_j^{U,L} \cdot i_{Cj}^{U,L}, \tag{1}$$

where $m_j^{U,L}$ are called the modulation indices of the upper and lower arms for all three phases. Values $v_{Cj}^{U,L}$ and $i_{Cj}^{U,L}$ are the voltages and currents of the upper and lower arm equivalent capacitances.

As mentioned before, the state-space modeling adopted in this work uses the $\Sigma - \Delta$ representation instead of commonly used *Upper-Lower* (*U-L*) form. More precisely, under the $\Sigma - \Delta$ nomenclature, it is possible to propose four state- and four control variables for the presented MMC topology. It is worthwhile mentioning that the Δ variables are associated with the fundamental angular frequency ω, and the third harmonic 3ω components. In comparison, the $\sum$ variables are associated with -2ω harmonics and contain a DC component.

For this converter's model, the aforementioned $\Sigma - \Delta$ variables in the upper and lower arms can be represented as follows [8],

$$\begin{aligned}
&v_{Cj}^{\Delta} = (v_{Cj}^{U} - v_{Cj}^{L}) \Big/ 2,\ v_{Cj}^{\sum} = (v_{Cj}^{U} + v_{Cj}^{L}) \Big/ 2,\\
&m_j^{\Delta} = m_j^{U} - m_j^{L},\ m_j^{\sum} = m_j^{U} + m_j^{L},\\
&v_{Mj}^{\Delta} = (-v_{Mj}^{U} + v_{Mj}^{L}) \Big/ 2 = -(m_j^{\Delta} v_{Cj}^{\sum} + m_j^{\sum} v_{Cj}^{\Delta}) \Big/ 2,\\
&v_{Mj}^{\sum} = (v_{Mj}^{U} + v_{Mj}^{L}) \Big/ 2 = (m_j^{\sum} v_{Cj}^{\sum} + m_j^{\Delta} v_{Cj}^{\Delta}) \Big/ 2.
\end{aligned} \tag{2}$$

For the MMC configuration in Fig. 1, we define the AC-gird currents dynamics i_j^{Δ} and circulating currents dynamics $i_j^{\sum}$ for three-phase as:

$$i_j^{\Delta} = i_j^{U} - i_j^{L},\ i_j^{\sum} = (i_j^{U} + i_j^{L}) \Big/ 2. \tag{3}$$

Applying the Kirchhoff voltage law (KVL) to the MMC equivalent circuit depicted in Fig. 1, we immediately obtain the grid currents and circulating currents dynamics as:

$$\begin{aligned}
&L_{eq}^{ac} \tfrac{d}{dt}(\vec{i}_j^{\Delta}) = \vec{v}_{Mj}^{\Delta} - R_{eq}^{ac} \vec{i}_j^{\Delta} - \vec{v}_j^{G},\\
&L_{arm} \tfrac{d}{dt}(\vec{i}_j^{\Sigma}) = \tfrac{v_{dc}}{2} - \vec{v}_{Mj}^{\Sigma} - R_{arm} \vec{i}_j^{\Sigma},
\end{aligned} \tag{4}$$

where, L_{eq}^{ac} and R_{eq}^{ac} are the equivalent inductor and resistor in the AC control loop, which can be expressed as $L_{eq}^{ac} = L_{arm}/2 + L_r$ and $R_{eq}^{ac} = R_{arm}/2 + R_r$, respectively. $\vec{v}_{Mj}^{\Delta}$ is the modulated voltage at the interfacing point between MMC and AC-grid side, and $\vec{v}_j^{G}$ are the balanced AC-grid voltages.

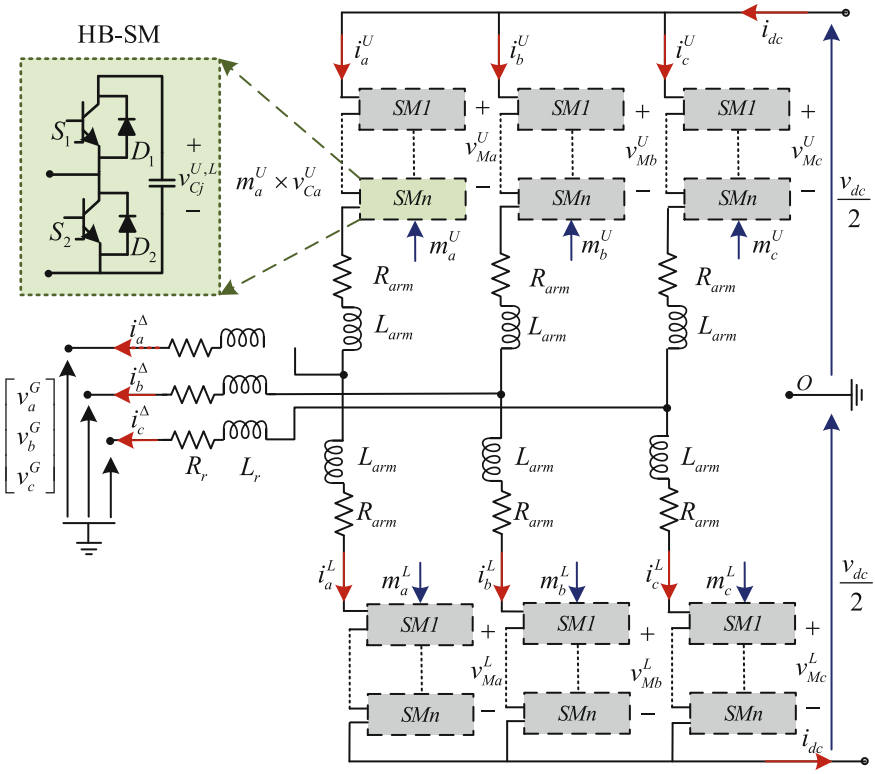

Fig. 1. Schematic diagram of MMC topology.

The Park's transformation and the inverse Park's transformation at ω angular frequency are applied to determine the dynamics of the state variables in d-q frame, which are given with formula as,

$$P_{n\omega}(t) = \frac{2}{3}\begin{bmatrix} \cos(n\omega t) & \cos(n\omega t - 2\pi/3) & \cos(n\omega t - 4\pi/3) \\ \sin(n\omega t) & \sin(n\omega t - 2\pi/3) & \sin(n\omega t - 4\pi/3) \\ \frac{1}{2} & \frac{1}{2} & \frac{1}{2} \end{bmatrix},$$
$$P_{n\omega}^{-1}(t) = \frac{3}{2}P_{n\omega}^{T}(t) + \frac{1}{2}\begin{bmatrix} 0 & 0 & 1 \\ 0 & 0 & 1 \\ 0 & 0 & 1 \end{bmatrix}, \tag{5}$$

where $n = 1$ for the "Δ" variables, whereas $n = 2$ for the "$\sum$" variables.

By Park's transformation, one can obtain the dynamics of grid current $\vec{i}_{dq}^{\Delta}$ and circulating currents:

$$\begin{aligned} \frac{d}{dt}(\vec{i}_{dq}^{\Delta}) &= \frac{1}{L_{eq}^{ac}}(\vec{v}_{Mdq}^{\Delta} - (\omega L_{eq}^{ac} J_2 + R_{eq}^{ac} I_2)\vec{i}_{dq}^{\Delta} - \vec{v}_{dq}^{G}), \\ \frac{d}{dt}(\vec{i}_{dq}^{\sum}) &= -\frac{1}{L_{arm}}(\vec{v}_{Mdq}^{\sum} + (R_{arm} I_2 - 2\omega L_{arm} J_2)\vec{i}_{dq}^{\sum}), \end{aligned} \tag{6}$$

where, $\vec{v}_{Mdq}^{\Delta}$ and $\vec{v}_{Mdq}^{\sum}$ are the modulated voltages in grid current controller and circulating current controller, respectively. I_2 is the identity matrix with size 2×2, and J_2 is defined as:

$$J_2 = \begin{bmatrix} 0 & 1 \\ -1 & 0 \end{bmatrix}. \tag{7}$$

3 Modeling of the Proposed Adaptive Backstepping Control

This section covers the modeling of the MMC's output current controlling loop utilizing the proposed adaptive BSC methods. Furthermore, the *Lyapunov* stability analysis is provided as a measure of the system's stability.

3.1 Output Current Control

This control layer contains two control targets, which are the *d-q* frame grid currents i_d^{Δ} and i_q^{Δ}. It is worthwhile to highlight that the energy stored in the capacitor of each MMC's sub-module can be used as an exchanged energy between the DC and AC sides and provide a virtual reference for the state variable i_d^{Δ}. Therefore, the state variables vector $\vec{x}$ and control variables vector $\vec{u}$ can be defined as follows,

$$\begin{aligned} \vec{x} &= \begin{bmatrix} x_1 & x_2 & x_3 \end{bmatrix}^T = [\, W_z \; i_d^{\Delta} \; i_q^{\Delta} \,]^T, \\ \vec{u} &= \begin{bmatrix} u_1 & u_2 \end{bmatrix}^T = \begin{bmatrix} v_{Md}^{\Delta} & v_{Mq}^{\Delta} \end{bmatrix}^T, \end{aligned} \tag{8}$$

where W_z represents the sum of the stored energy in SMs and can be calculated as $W_z = 3C(V_{dc})^2 \big/ N$, and C is the capacitance of each sub-module.

Then, the MMC's dynamics described in Sect. 2 can be presented as,

$$\begin{aligned} \dot{x}_1 &= P_{ac} - P_{dc} = \tfrac{3}{2} u_d^G i_d^{\Delta} - P_{dc}, \\ \dot{x}_2 &= \frac{1}{L_{eq}^{ac}}(v_{Md}^{\Delta} - R_{eq}^{ac} i_d^{\Delta} - \omega L_{eq}^{ac} i_q^{\Delta} - v_d^G), \\ \dot{x}_3 &= \frac{1}{L_{eq}^{ac}}(v_{Mq}^{\Delta} - R_{eq}^{ac} i_q^{\Delta} + \omega L_{eq}^{ac} i_d^{\Delta} - v_q^G). \end{aligned} \tag{9}$$

To analyze the system *Lyapunov* stability, the error variables $\boldsymbol{e}$ and their time derivatives are defined as follows,

$$\begin{aligned} \boldsymbol{e} &= \begin{bmatrix} e_1 & e_2 & e_3 \end{bmatrix}^T = \begin{bmatrix} W_{zref} - W_z & e_v - x_2 & e_3 - x_3 \end{bmatrix}^T, \\ \dot{\boldsymbol{e}} &= \begin{bmatrix} \dot{e}_1 & \dot{e}_2 & \dot{e}_3 \end{bmatrix}^T = \begin{bmatrix} \dot{W}_{zref} - \dot{W} & \dot{e}_v - \dot{x}_2 & \dot{e}_3 - \dot{x}_3 \end{bmatrix}^T, \end{aligned} \tag{10}$$

where e_v is the virtual control variable, which corresponds to the desired value of the state variable x_2.

Now let us define the following *Lyapunov* function:

$$\mathrm{V}(x) = \frac{1}{2}e_1^2 + \frac{1}{2}e_2^2 + \frac{1}{2}e_3^2. \tag{11}$$

It is straightforward to conclude that $\mathrm{V}(x)$ is positive for all $e_1,\ e_2,\ e_3 \neq 0$, and $\mathrm{V}(x) = 0$ is met only in the condition that $e_1,\ e_2,\ e_3 = 0$, which means that the system is operating in a steady-state. According to Lyapunov's direct method [10], the transient stability analysis is used to determine whether the *Lyapunov* function is decreasing along the system's trajectories. Given that the constructed *Lyapunov* function is differentiable everywhere, we need to prove that the time derivative of *Lyapunov* function is negative everywhere except in the origin (steady-state) where it is zero.

The negative derivatibe $\dot{\mathrm{V}}(x)$ can be expressed as follows,

$$\dot{\mathrm{V}}(x) = e_1\dot{e}_1 + e_2\dot{e}_2 + e_3\dot{e}_3. \tag{12}$$

Let us first consider the item $e_1\dot{e}_1$. The $\dot{e}_1$ can be expressed as $\dot{e}_1 = \dot{W}_{zref} - 3v_d^G i_d^\Delta \big/ 2 + P_{dc}$ according to Eq. (9). Notice that the W_{zref} is a constant, which gives its derivative $\dot{W}_{zref}$ being 0. To ensure $e_1\dot{e}_1$ is strictly negative, we can define the item $\dot{e}_1$ as $-k_1e_1$. Thus, the desired value of i_d^Δ, which refers to the variable e_v, should be:

$$e_v = 2(k_1e_1 + P_{dc}) \Big/ 3v_d^G. \tag{13}$$

Therefore, $e_1\dot{e}_1$ is always negative and can be expressed as $-k_1e_1^2$ for $k_1 > 0$, where one can obtain:

$$\begin{aligned}\dot{\mathrm{V}}(x) &= e_1(-3v_d^G(e_v - e_2) \big/ 2 + P_{dc}) + e_2\dot{e}_2 + e_3\dot{e}_3 \\ &= -k_1e_1^2 + e_2(\dot{e}_2 - 3e_1v_d^G \big/ 2) + e_3(\dot{i}_{qref}^\Delta - (v_{Mq}^\Delta - R_{eq}^{ac}i_q^\Delta + \omega L_{eq}^{ac}i_d^\Delta - v_q^G) \Big/ L_{eq}^{ac})\end{aligned} \tag{14}$$

If the following conditions are satisfied and we guarantee that k_2,$k_3 > 0$, then $\dot{\mathrm{V}}(x) < 0$ if:

$$\begin{aligned}&\dot{e}_2 - 3e_1v_d^G \big/ 2 = -k_2e_2, \\ &\dot{i}_{qref}^\Delta - (v_{Mq}^\Delta - R_{eq}^{ac}i_q^\Delta + \omega L_{eq}^{ac}i_d^\Delta - v_q^G) \Big/ L_{eq}^{ac} = -k_3e_3.\end{aligned} \tag{15}$$

Up to this point, we have proved the time derivative of *Lyapunov* function is strictly negative everywhere, which can be expressed as: $\dot{\mathrm{V}}(x) = -k_1e_1^2 - k_2e_2^2 - k_3e_3^2 < 0$. The control variables v_{Md}^Δ and v_{Mq}^Δ are then:

$$\begin{aligned}v_{Md}^\Delta &= L_{eq}^{ac}(\dot{i}_{dref}^\Delta + k_2e_2 - 3e_1v_d^G \big/ 2) + R_{eq}^{ac}i_d^\Delta + \omega L_{eq}^{ac}i_q^\Delta + v_d^G, \\ v_{Mq}^\Delta &= (\dot{i}_{qref}^\Delta + k_3e_3)L_{eq}^{ac} + R_{eq}^{ac}i_q^\Delta - \omega L_{eq}^{ac}i_d^\Delta + v_q^G.\end{aligned} \tag{16}$$

However, when the system is subjected to AC/DC faults or sudden changes of active/reactive power, the angular frequency ω of the AC system will be affected to

some extent, which affects the accuracy of the *Lyapunov* function and affects the tracking ability of the BSC controller. Therefore, adaptive control is introduced in our work. We can use the estimated value $\hat{\omega}_{dq}$ as the adaptive rate of the system frequency to replace ω. The corresponding tracking errors of the frequency ω can be defined as:

$$e_{\omega dq} = \omega - \hat{\omega}_{dq},\ \dot{e}_{\omega dq} = \dot{\omega} - \dot{\hat{\omega}}_{dq}, \tag{17}$$

where $\dot{\omega}$ is considered 0 in this paper. This gives the new condition for v_{Md}^{Δ} and v_{Mq}^{Δ}:

$$\begin{aligned} v_{Md}^{\Delta} &= L_{eq}^{ac}(\dot{i}_{dref}^{\Delta} + k_2 e_2 - 3e_1 v_d^G / 2) + R_{eq}^{ac} i_d^{\Delta} + \hat{\omega} L_{eq}^{ac} i_q^{\Delta} + v_d^G, \\ v_{Mq}^{\Delta} &= (\dot{i}_{qref}^{\Delta} + k_3 e_3) L_{eq}^{ac} + R_{eq}^{ac} i_q^{\Delta} - \hat{\omega} L_{eq}^{ac} i_d^{\Delta} + v_q^G. \end{aligned} \tag{18}$$

Then, the time derivative of the updated *Lyapunov* function can be expressed as,

$$\begin{aligned} \dot{\mathrm{V}}(x) =& e_1\dot{e}_1 + e_2\dot{e}_2 + e_3\dot{e}_3 + e_{\omega d}\dot{e}_{\omega d} + e_{\omega q}\dot{e}_{\omega q} \\ =& -k_1 e_1^2 - k_2 e_2^2 - k_3 e_3^2 + e_2(\hat{\omega}_d - \omega) L_{eq}^{ac} i_q^{\Delta} + e_{\omega d}\dot{e}_{\omega_d} + e_3(\hat{\omega}_q + \omega) L_{eq}^{ac} i_d^{\Delta} + e_{\omega q}\dot{e}_{\omega_q} \\ =& -k_1 e_1^2 - k_2 e_2^2 - k_3 e_3^2 - e_{\omega}(\dot{\hat{\omega}}_d + e_2 L_{eq}^{ac} i_q^{\Delta}) - e_{\omega}(\dot{\hat{\omega}}_q - e_3 L_{eq}^{ac} i_d^{\Delta}). \end{aligned} \tag{19}$$

In this case, we can make sure that the items $\dot{\hat{\omega}}_d + e_2 L_{eq}^{ac} i_q^{\Delta}$ and $\dot{\hat{\omega}}_q - e_3 L_{eq}^{ac} i_d^{\Delta}$ are zero. Thus, the derivative $\dot{\mathrm{V}}(x)$ is negative semi-definte (NSD), which is $\dot{\mathrm{V}}(x) \leq 0$, where one can obtain that:

$$\hat{\omega}_d = -\int e_2 L_{eq}^{ac} i_q^{\Delta} dt,\ \hat{\omega}_q = \int e_3 L_{eq}^{ac} i_d^{\Delta} dt. \tag{20}$$

Up to this point, the instability brought by the transient frequency of the system ω has been eliminated. To further eliminate the steady-state errors, additional adaptive terms θ_d and θ_q are considered [1], which can be expressed as,

$$\theta_d = -k_{di} \int e_2 dt,\ \theta_q = -k_{qi} \int e_3 dt, \tag{21}$$

where the k_{di} and k_{qi} are the control gains of the adaptive terms. It is noted that all adaptive terms would be zero in the steady-state.

With the adaptive terms, the BSC method can bring the system to a new steady-state with fewer overshoots and undershoots. Therefore, the control variables v_{Md}^{Δ} and v_{Mq}^{Δ} with the proposed adaptive BSC method are obtained:

$$\begin{aligned} v_{Md}^{\Delta} &= L_{eq}^{ac}(\dot{i}_{dref}^{\Delta} + k_2 e_2 - 3e_1 v_d^G / 2) + R_{eq}^{ac} i_d^{\Delta} - L_{eq}^{ac} i_q^{\Delta} (\int e_2 L_{eq}^{ac} i_q^{\Delta} dt) + v_d^G \theta_d - k_{di} \int e_2 dt, \\ v_{Mq}^{\Delta} &= (\dot{i}_{qref}^{\Delta} + k_3 e_3) L_{eq}^{ac} + R_{eq}^{ac} i_q^{\Delta} - L_{eq}^{ac} i_d^{\Delta} (\int e_3 L_{eq}^{ac} i_d^{\Delta} dt) + v_q^G - k_{qi} \int e_3 dt. \end{aligned} \tag{22}$$

The OCC is carefully designed and its design guarantees stability because the time derivative of *Lyapunov* function $\dot{\mathrm{V}}(x)$ is strictly negative.

3.2 Other Controlling Loops

Since the BSC method is more suitable for higher-order systems, the circulating current suppression controller (CCSC) in this paper implements traditional PI control. The CCSC is constructed to set the circulating current to its reference, which is assumed to be $\vec{i}^{\Sigma}_{dq,ref} = [0\,0]^T$. The specific equations of CCSC adopted in this paper are presented as follows [6],

$$\begin{aligned} \dot{\vec{\xi}}^{\Sigma}_{dq} &= \vec{i}^{\Sigma}_{dq,ref} - \vec{i}^{\Sigma}_{dq}, \\ \vec{v}^{\Sigma}_{Mdq,ref} &= -K^{\Sigma}_{I}\vec{\xi}^{\Sigma}_{dq} - K^{\Sigma}_{P}(\vec{i}^{\Sigma}_{dq,ref} - \vec{i}^{\Sigma}_{dq}) + 2\omega L_{arm} J_2 \vec{i}^{\Sigma}_{dq}, \end{aligned} \tag{23}$$

where the proportional gain K_P is set to 0.8 p.u., the integral gain K_I is set to 0.0125 p.u. [6] in this paper.

The reference value $i^{\Delta}_{q,ref}$ for the q-axis grid current is provided by variation of the reactive power Q_{ac} of AC gird. The reactive power control can be designed using the equations as follows,

$$\begin{aligned} \dot{\xi}_Q &= Q_{ac,ref} - Q_{ac}, \\ i^{\Delta}_{q,ref} &= -K_{P,Q}(Q_{ac,ref} - Q_{ac}) + K_{I,Q}\xi_Q, \end{aligned} \tag{24}$$

where the K_P and K_I are the control gain of the reactive power controller.

Up to this point, the overall control scheme for the MMC is described in Fig. 2.

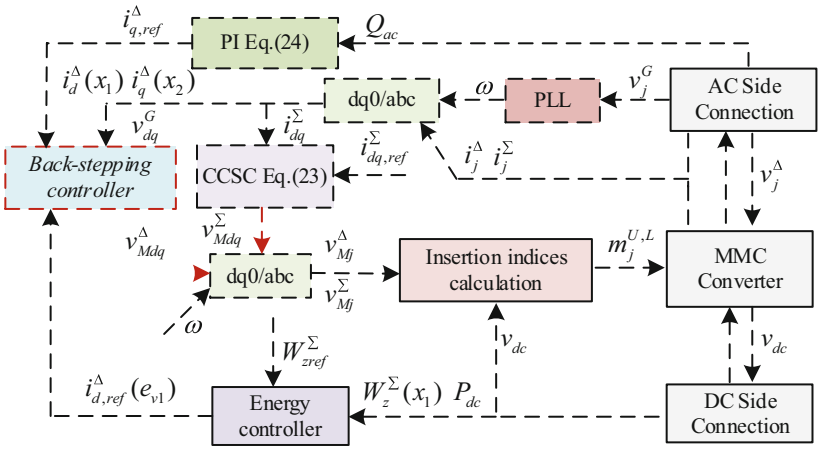

Fig. 2. Schematic diagram of a back-stepping controller for MMC.

4 Studied HVDC Digital Twin

To demonstrate the capabilities of the proposed adaptive BSC method, a point-to-point ±525 kV HVDC system is modeled in the RTDS test platform as a digital twin. The configuration of the system is given in Fig. 3.

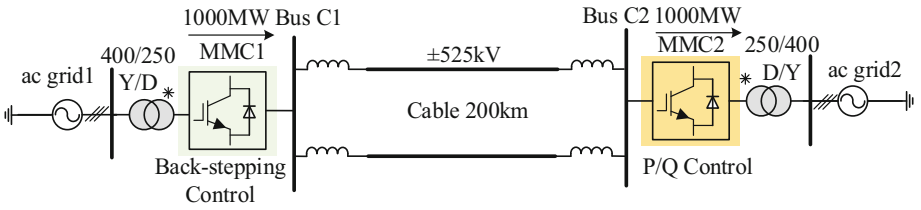

Fig. 3. Topology of the HVDC digital twin

Among the different models provided in RSCAD, the "rtds_vsc_MMC5" model is specified to evaluate the proposed controller in this paper. The chosen MMC RSCAD model is the Average Arm Model (AAM) with H-bridge configuration [9]. The specified model is suitable for testing outer control strategies [5]. The model consists of the automatic balancing algorithm for submodule capacitor voltages, which runs a small time-step between 1.2–1.5 μs.

The AC grid is linked with the MMC through a star/delta transformer, where the AC grid1 is working as sending end with nominal active power of 1000 MVA and AC grid2 as the receiving end. The AC transformer's star point is solidly grounded. The parameter rating of the transformer can be seen in Table 1. The series current limiting inductors are positioned at the outlets of DC cable lines, with the same inductance of 120 mH. The sampling frequency is standardized as 96 kHz following the recommendation of IEC 61869-9 1 [1]. The detailed parameters and nominal values of the studied HVDC digital twin are given in Table 1.

Table 1. Parameters of point-to-point MMC-HVDC verification system

Item	MMC1	MMC2
Rated active power/MW	1000	1000
Nominal DC voltage/kV	±525	±525
Nominal frequency/Hz	60	60
Transformer ratio (Yg/D)	400/250	400/250
Transformer reactance/pu	0.18	0.18
Number of SMs per arm	512	512
Arm resistance/Ω	0.08	0.08
Arm reactor/mH	0.042	0.042
DC inductor/mH	120	120

In this paper, only MMC1 is simulated with the proposed BSC method and taken as the studied converter in the analysis. The MMC2 is regulated using classical PI controllers with an active/reactive power control strategy. The control modes of each MMC converter and control gains of the studied system are presented in Table 2.

Table 2. Control mode and parameters of converters

Converter	Control mode	Parameters
MMC1	Adaptive back-stepping control (p.u.)	$K_1 = 13$
		$K_2 = 10\ K_{di} = 0.01$
		$K_3 = 5\ K_{qi} = 0.125$
	Q-control (p.u.)	$K_P = 2.0\ K_I = 0.3$
MMC2	P-control (p.u.)	$K_P = 2.0\ K_I = 0.15$
	Q-control (p.u.)	$K_P = 2.0\ K_I = 0.3$

5 Effectiveness of the Proposed Control Method

In this section, we present the simulation results when the proposed BSC method is applied for the control of MMC. In addition, we compare the transient response of the proposed adaptive BSC with the classical PI methods to illustrate the major contribution of this paper. For a typical application of the HVDC system, active and reactive power reference signals are requested to be constant in a steady state. The test case carried out in the RTDS environment is the step change in active power from 0 p.u. to 0.5 p.u. at $t_0 = 0.2$ s and increases to 0.7 p.u. at $t_1 = 1.2$ s.

The detailed results are presented in Figs. 4 and 5. Figure 4(a) provides the results of energy controller. The capacitor energy W_z initials at 0.9 p.u. since the active power equals zero at this time instance. At the instant $t = t_0$, the active power reference experiences a step increase to 0.5 p.u., the SM capacitors of MMC1 start to charge, and the energy W_z gradually increases to the rated value. During the two-step changes, W_z is always comprised near the reference value, and hence, no energy overshoots are noticeable, which demonstrates the desired ability of the energy controller of delivering a precise reference signal to the d-axis gird current. Figure 4(b) is a good illustration of the tracking performance of i_d^{Δ} and its virtual reference signal e_{v1}. It is concluded that the current i_d^{Δ} and error e_{v1} are well controlled during these transients at the time instances t_0 and t_1, which completely overlap with each other without perceptible undershoots or overshoots. This constitutes the strength of the proposed BSC method, as the fast response is ensured for the grid currents. The entire transient process of each step changes only last for 10 ms. According to Fig. 4(b), the results strongly confirm the BSC method's superiority over the PI controller in control accuracy and tracking speed. Figure 4(c) provides the results of the q-axis current i_q^{Δ} and its reference signal i_{qref}^{Δ}. Due to the decoupling control design, the step changes in active power will not cause a significant impact on i_q^{Δ}, and after a short transient process, i_q^{Δ} is tuned in alignment with its rated value. Since the reference signal for the q-axis current is provided by the upper reactive power controller, the BSC method has similar results with the PI control. The simulation results of control variables can be observed in Fig. 4(d). The active power step-changes at the time instants t_0 and t_1 will not cause noticeable changes in voltages v_{Md}^{Δ} and v_{Mq}^{Δ}, and their values are equal to rated values.

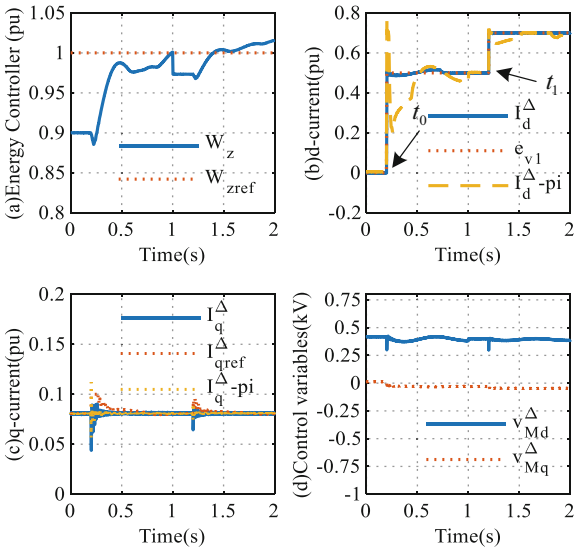

Fig. 4. Simulation results. (a) Energy controller (b) *d*-axis current (c) *q*-axis current (d) Control variables.

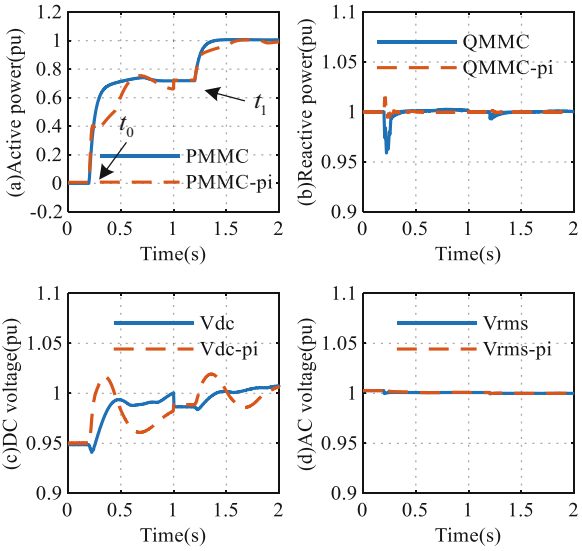

Fig. 5. Simulation results. (a) Active power (b) Reactive power (c) DC side voltage (d) AC grid voltage.

Figure 5(a) provides the active power on the AC grid, which has initial value 0 p.u and increases smoothly to the new steady-state without the phenomenon of oscillations and overshoots. However, it is obvious that the transient response of active power controlled by PI is slower and contains noticeable oscillations, which is caused by the inaccurate

control of i_d^{Δ} presented in Fig. 5(b). The reactive power presented in Fig. 5(b) only exhibits a small decay at the instant of step-change and restores to 1 p.u. promptly. It is also marked that the DC voltage in Fig. 5(c) is aligned with the trends of active power, the value is always around the 1 p.u., and the BSC method causes smaller fluctuations. The Root-Mean-Square (RMS) value of AC gird observed in Fig. 5(d) is less affected by the step changes of active power, and hence, no saturation effects are evident.

In Fig. 6, the steady state operation during time interval 1.8 s–1.85 s is presented. It is observed that all the values of errors variables and *Lyapunov* function are clearly very small during the operation in steady state, which shows the accuracy of the designed controller.

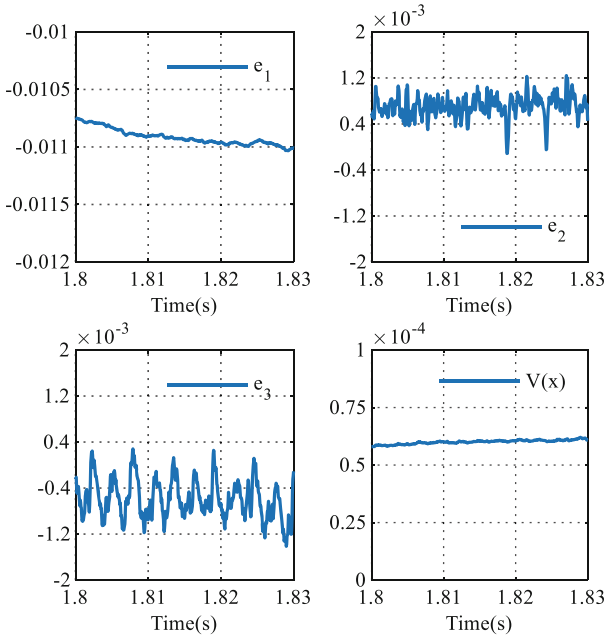

Fig. 6. Simulation results. (a) Error e_1 (b) Error e_2 (c) Error e_3 (d) *Lyapunov* function.

6 Conclusion

In this article, a non-linear control strategy relying on an adaptive BSC method was proposed. The *Lyapunov* theory is applied to stabilize the MMC's operation with several strict-feedback structures. These feedback structures include DC voltage, reactive power, and MMC arm capacitor energy controllers. To simplify the controller designing, the *abc* frame is transformed into decoupled *d-q* representation, which simplifies the proposed approach. A virtual control parameter is designed as the reference signal for the *d*-axis grid current, which is provided by the upper layer energy controller. Numerous simulations are carried out in the RTDS simulation environment for determining the

control laws. The proposed adaptive BSC method is comprehensively evaluated for a classic point-to-point HVDC power system digital twin. In addition, the robustness of the proposed BSC method was precisely evaluated through a specific transient case. The results strongly support the superiority of the control strategy in stabilizing the MMC operation during transients.

References

1. Zhao, X., Li, K.: Adaptive backstepping droop controller design for multi-terminal high-voltage direct current systems. IET Gener. Transm. Distrib. **9**(10), 975–983 (2015)
2. Ahmadijokani, M., et al.: A back-stepping control method for modular multilevel converters. IEEE Trans. Ind. Electron. **68**(1), 443–453 (2021)
3. Perez, M.A., Bernet, S., Rodriguez, J., Kouro, S., Lizana, R.: Circuit topologies, modeling, control schemes, and applications of modular multilevel converters. IEEE Trans. Power Electron. **30**(1), 4–17 (2015)
4. Harnefors, L., et al.: Dynamic analysis of modular multilevel converters. IEEE Trans. Ind. Electron. **60**(7), 2526–2537 (2013)
5. Guide for the developments of models for HVDC converters in a HVDC grid. CIGRÉ Working Group B4.57, Paris (2014)
6. Shetgaonkar, A., Lekić, A., et al.: Microsecond enhanced indirect model predictive control for dynamic power management in MMC units. Energies **14**(11), 3318–3344 (2021)
7. Jin, Y., Xiao, Q., Jia, H., et al.: A dual-layer back-stepping control method for Lyapunov stability in modular multilevel converter based STATCOM. IEEE Trans. Ind. Electron **69**(3), 2166–2179 (2022)
8. Bergna-Diaz, G., Freytes, J., Guillaud, X., et al.: Generalized voltage-based state-space modeling of modular multilevel converters with constant equilibrium in steady state. IEEE J. Emerg. Sel. Top. **6**(2), 707–725 (2018)
9. Real-Time-Digital-Simulator: VSC small time-step modelling. Technical report, RTDS Technologies, Winnipeg, MB, Canada, October 2006
10. Shuai, Z., Shen, C., et al.: Transient angle stability of virtual synchronous generators using Lyapunov's direct method. IEEE Trans. Smart Grid **10**(4), 4648–4661 (2019)